

## First Results for Uranium Nitride Fuel Characterization Using an Accelerated Fuel Qualification Process

Zachary Miller , Landon Johnson , Lorena Alzate-Vargas , Jason Rizk , Christopher Matthews , Michael W. D. Cooper , Vedant Mehta , David A. Andersson , Galen T. Craven , Massimiliano Fratoni & Alex Levinsky

**To cite this article:** Zachary Miller , Landon Johnson , Lorena Alzate-Vargas , Jason Rizk , Christopher Matthews , Michael W. D. Cooper , Vedant Mehta , David A. Andersson , Galen T. Craven , Massimiliano Fratoni & Alex Levinsky (27 Oct 2025): First Results for Uranium Nitride Fuel Characterization Using an Accelerated Fuel Qualification Process, Nuclear Science and Engineering, DOI: [10.1080/00295639.2025.2567814](https://doi.org/10.1080/00295639.2025.2567814)

**To link to this article:** <https://doi.org/10.1080/00295639.2025.2567814>



Published online: 27 Oct 2025.



Submit your article to this journal 



Article views: 97



View related articles 



View Crossmark data   
CrossMark



# First Results for Uranium Nitride Fuel Characterization Using an Accelerated Fuel Qualification Process

Zachary Miller<sup>a,d</sup>, Landon Johnson<sup>c</sup>, Lorena Alzate-Vargas<sup>c</sup>, Jason Rizk<sup>b</sup>, Christopher Matthews<sup>b</sup>, Michael W. D. Cooper<sup>b</sup>, Vedant Mehta<sup>a</sup>, David A. Andersson<sup>b</sup>, Galen T. Craven<sup>c</sup>, Massimiliano Fratoni<sup>d</sup>, and Alex Levinsky<sup>a</sup>

<sup>a</sup>*Nuclear Engineering and Nonproliferation Division, Los Alamos National Laboratory (LANL), Los Alamos, NM;* <sup>b</sup>*Material Science and Technology Division, Los Alamos National Laboratory (LANL), Los Alamos, NM;* <sup>c</sup>*Theoretical Division, Los Alamos National Laboratory (LANL), Los Alamos, NM;* <sup>d</sup>*Department of Nuclear Engineering, University of California, Berkeley, CA*

Received August 13, 2024

Accepted for Publication September 22, 2025

**Abstract** — *Traditional nuclear fuel qualification is a lengthy process challenged by erratic or incomplete irradiation experimental data, leading to many unqualified fuels. In response, this paper presents an accelerated fuel qualification (AFQ) framework that integrates multiscale modeling, machine learning, and legacy data assimilation to inform specific integral testing. The framework leverages atomistic simulations to elucidate fundamental mechanisms, such as xenon diffusion and defect kinetics, which inform mechanistic models of fuel behavior. These mechanistic models are then validated against legacy experimental data, while machine learning is used to refine critical parameters, such as Xe diffusivity, and to further reduce computational uncertainties.*

*As a demonstration, the framework is applied to characterize uranium mononitride (UN) fuel, resulting in the quantification of swelling, which is a dominant failure mechanism, uncertainty quantification of the swelling process in UN, and the development of performance envelopes as a function of temperature, linear heat generation rate, and burnup. The AFQ methodology outlined here offers a robust proof-of-concept template for qualifying advanced nuclear fuels, supporting regulatory modernization efforts for next-generation reactor technologies.*

**Keywords** — *Accelerated fuel qualification, uranium nitride, fuel performance, BISON, mechanistic model.*

## I. INTRODUCTION

Many new reactor designs for both terrestrial and space applications are targeting challenging operating regimes, such as high temperature, long lifespan, and high burnup. These designs also aim for compact size, enhanced reactor safety, and sufficient safety margins covering all operating conditions. As a result, there is a need to use nuclear fuels that can support these ambitious goals. Uranium mononitride (UN) has emerged as a promising candidate, offering high thermal conductivity, a high melting point, chemical compatibility with most cladding materials, and high fissile density [1]. UN is suitable for both fast and thermal spectrum reactors, making it attractive for a wide range of designs.

However, before any nuclear fuel can be used in commercial or advanced applications, it must be qualified and approved by the U.S. Nuclear Regulatory Commission (NRC). Research and development on UN began in the 1960s, primarily for space and generation-IV (GEN-IV) reactor applications. Several programs successfully characterized the properties of unirradiated UN and conducted limited irradiation and post-irradiation examinations. While these efforts generated valuable data, the available information remains insufficient compared to that of traditional fuels (i.e.,  $UO_2$ ), and funding for further experimental programs was discontinued before the fuel qualification could be completed.

To support the qualification of advanced fuels and the licensing of advanced reactor technologies, the NRC began looking at the criteria and possible alternative frameworks. The accelerated fuel qualification (AFQ) process, discussed

by the NRC, is of particular interest to vendors aiming to deploy advanced reactors by the end of this decade. The AFQ process is designed to reduce the number of required integral irradiation tests by supplementing existing experimental data with advanced, physics-based modeling and simulation [2].

In this paper, we describe the development of an AFQ approach that couples advanced modeling and simulation methods, machine learning (ML), and legacy data from the past experiments. The framework is demonstrated on a proof-of-concept UN fuel characterization.

## II. PROPOSED AFQ FRAMEWORK

The proposed AFQ framework couples legacy experimental data with advanced modeling and simulation, ML, and a limited number of targeted experiments focused on investigating areas of high uncertainty. A graphical outline of the approach is shown in Fig. 1. This tightly coupled, multiscale methodology ensures that each component informs and enhances the others.

Atomic-scale defects (e.g., such as vacancies, interstitials) drive macroscopic fuel degradation mechanisms, such as volumetric swelling, fission gas release, and creep [3]. Such degradation directly threatens key reactor safety functions, including the confinement of radioactive materials, control of reactivity, and effective core cooling.

To accurately predict these phenomena, the framework integrates atomistic simulations, including density

functional theory (DFT) and ML interatomic potentials, to compute defect diffusion rates and cluster growth kinetics [3–7]. The results of the atomistic simulations, e.g., the entropy and enthalpy of structural defects, are scaled up to the mesoscopic regime via cluster dynamics simulations to predict diffusion coefficients. ML models trained on experimental data, cluster dynamics outputs, and data-augmented experimental legacy data sets predict material properties, such as diffusion coefficients, without the need for computationally intensive molecular simulations [3].

ML also refines interatomic potentials, such as those for uranium, derived from atomic-scale calculations, thereby improving the fidelity of the simulations that investigate radiation, chemical, and manufacturing effects. These enhanced potentials are subsequently used to parameterize mechanistic fuel performance models, closing the multiscale loop and significantly reducing the experimental burden required for fuel qualification.

Uncertainty quantification (UQ) is critical for ensuring model validity and acceptability. Unlike empirical models with a limited domain of applicability, our mechanistic approach uses first-principles parameters, such as grain size, defect density, and porosity, for example [3,8,9]. Mechanistic fuel performance models describe the interactions of these microstructure state variables as a function of reactor operational conditions and irradiation time, predicting consequent changes in the fuel, and therefore the surrounding materials, such as cladding.

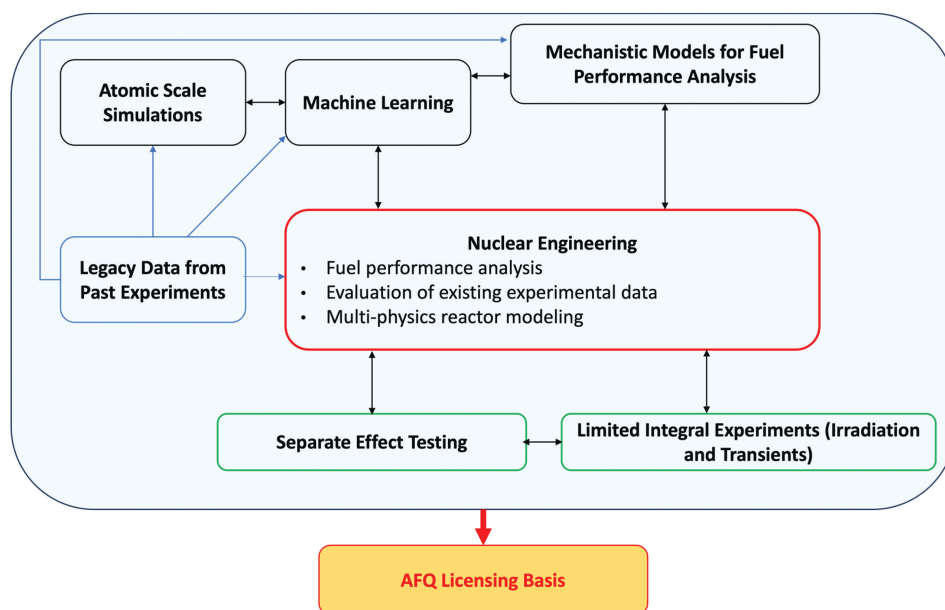


Fig. 1. Proposed AFQ approach.

However, the accuracy of these predictions depends on rigorous UQ. We employ advanced statistical methods and ML–driven sensitivity analysis to identify and reduce the impact of key uncertainties on swelling and other fuel performance predictions. This process enhances the validity and robustness of the models, especially when extrapolating beyond existing experimental data.

A proof-of-concept demonstration of the proposed AFQ framework was developed by applying it to UN fuel, with the goal of reducing uncertainties related to the modeling and simulation of the physical phenomena that are the major contributors to safety limits and margins for nuclear fuels, and defining a preliminary fuel performance envelope. Fuel swelling is identified as the governing life-limiting [10,11] mechanism for UN fuel, and the initial fuel performance envelope is defined based on fuel swelling as a function of fuel temperature, linear heat generation rate, and burnup (neutron fluence). The envelope maps the parameter space where mechanistic fuel performance code predictions align with experimental data, and it serves as the starting point for reactor design and future qualification experiments.

Vendors can expand this envelope using phenomena identification and ranking table (PIRT) analysis and targeted experiments, leveraging the AFQ framework to prioritize high-impact tests and refine safety margins for specific reactor designs. Moreover, the workflow presented here is not specific to swelling in UN fuel and can be transferred to various other physical behaviors and to other fuels.

With the AFQ framework and its application to UN fuel established, the next section presents the combined development and validation of the mechanistic models and ML approaches. Here, ML-driven refinement of key parameters, such as diffusivity coefficients, directly feeds into mechanistic fuel performance simulations (e.g., in BISON [12]), supporting UQ and enabling more reliable predictions of swelling and related phenomena. This integration ensures that the mechanistic models are both physically grounded and statistically credible, providing a solid foundation for defining the initial fuel performance envelope and supporting future experimental campaigns.

Finally, legacy data and these validated models will define the performance envelope, specifying operational limits for temperature, linear heat generation rate, and burnup, where mechanistic predictions align with experimental data. This envelope serves as the foundation for reactor designers to expand via targeted PIRT-guided experiments.

### III. ML-ENHANCED MECHANISTIC MODELING FOR URANIUM NITRIDE SWELLING PREDICTION AND UNCERTAINTY REDUCTION

As mentioned, our AFQ methodology is focused on reducing uncertainties in advanced fuel performance modeling. Our recommended approach is shown in [Fig. 2](#). The process begins with an assessment of initial uncertainties, informed by legacy experimental data and current UN empirical models. These models employ swelling correlations developed by Ross et al. [13] for space nuclear applications, based largely on the SNAP-50 experimental campaign. However, these correlations have a limited domain of applicability (fuel temperature: 1200 to 1600 K and burnup: 0.05 to 4.58 at. %) and exhibit projected uncertainties of  $\pm 25\%$  at burnups above 1.12% fissions per initial metal atom (FIMA) and greater than 60% at lower burnups [13].

Next, the AFQ process leverages legacy data and new mechanistic BISON models, initially informed by atomistic simulations, to describe the interactions of all microstructure state variables as a function of reactor operational conditions and irradiation time. It is the goal of this step to begin model verification against the empirical model and experimental data.

Several UN fuel testing campaigns were conducted over the past 40 years, resulting in a limited number of experimental data sets reflecting UN fuel swelling as a function of fuel temperature, power density and burnup [14–37]. These campaigns, including SNAP-50 CANEL, SNAP-50 ORNL, BR-10, NASA and Battelle, primarily targeted high-temperature irradiation regimes, with most tests limited to burnups up to 5% FIMA. Only the BR-10 series extended this range to 5% to 8% FIMA, reflecting GEN-IV SMR designs. [Fig. 3](#) illustrates the available UN volumetric fuel swelling experimental data as a function of burnup, power density and temperature.

When comparing new fuel performance data with legacy data sets, it is essential to select data that are both reliable and well suited for accurate modeling. Consequently, the SNAP-50 test series was chosen as the ideal benchmark for this initial comparison. [Fig. 4](#) and [Table 1](#) provide a detailed comparison of the legacy empirical model, the new mechanistic model, and the experimental data from the SNAP-50 series, enabling a clear evaluation of model performance against established experimental results.

Despite the utility of these data, substantial uncertainties (4% to 67%) persist due to the limited number of tests and gaps that remain in the test documentation. The

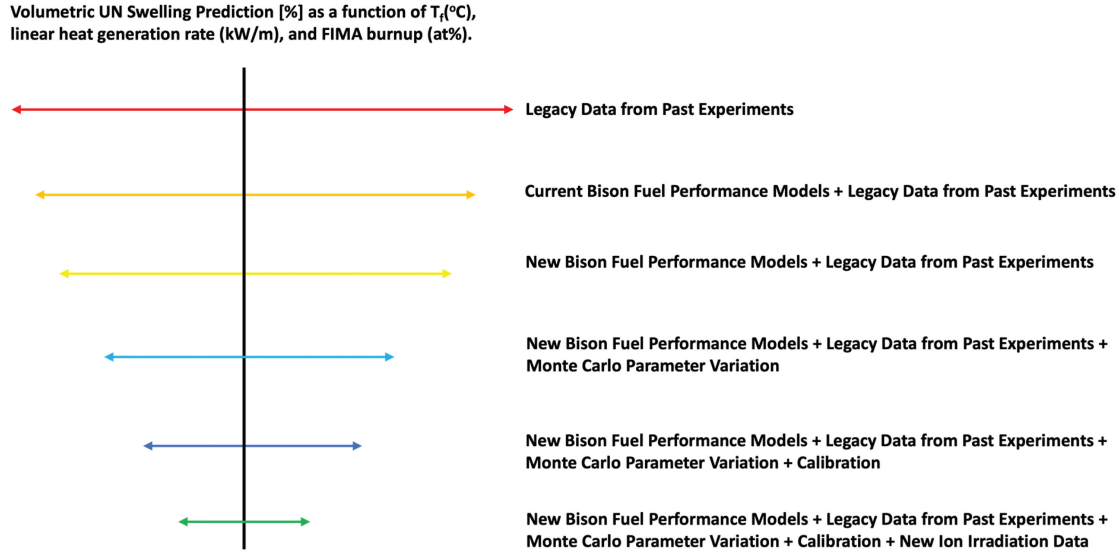


Fig. 2. Methodology of uncertainty reduction for UN swelling prediction. The width of the horizontal arrows represents the qualitative amount of uncertainty for each level.

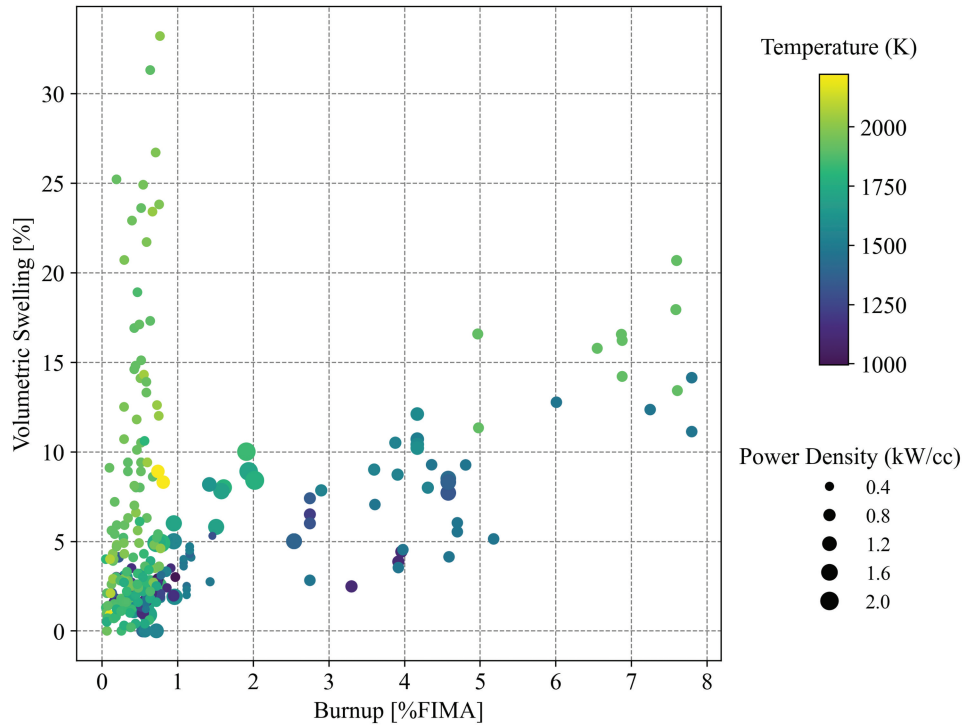


Fig. 3. UN fuel swelling as a function of burnup [14–37].

NRC has emphasized that legacy data used for fuel qualification must meet high quality assurance standards, necessitating their use alongside high-fidelity modeling and additional targeted experiments to support robust UN fuel qualification [2]. For this reason, careful consideration must be taken to select the appropriate legacy experimental data that will be used to compare our mechanistic

model against. For example, the top pin of test series 667 operated at a lower temperature compared to the middle and bottom pins, however, it shows that the swelling was nearly twice that of the middle and bottom pins. Generally, it is expected that lower temperatures cause less expansion within the fuel, leading to lower volumetric swelling.

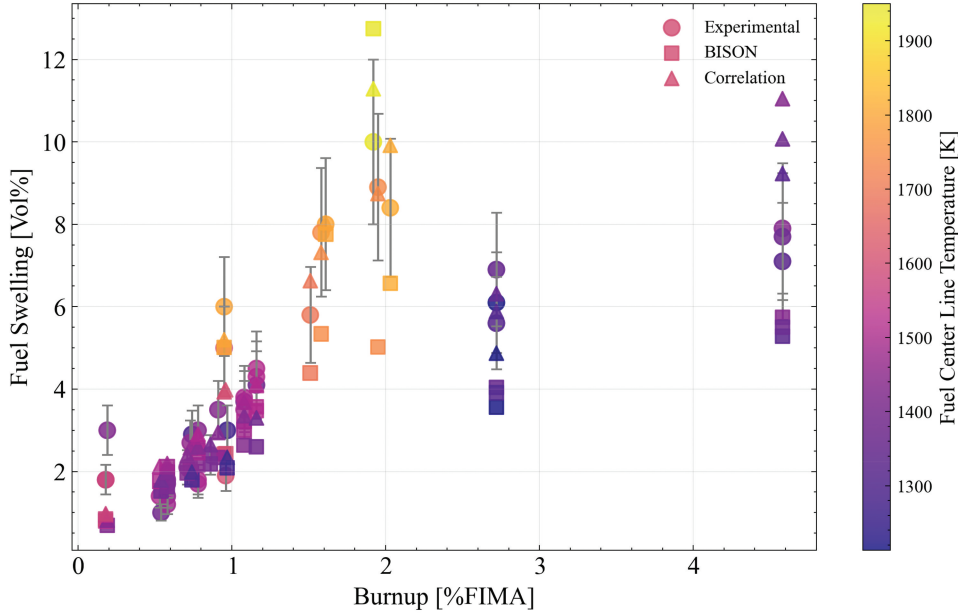


Fig. 4. Volumetric swelling versus burnup for various SNAP-50 test series. Error bars indicating  $\pm 20\%$  are included on all experimental data points [18,19].

As shown in Table 1, the mechanistic model demonstrated a clear performance advantage over the empirical correlation-based approach, reducing swelling prediction errors by 31% on average compared to the empirical correlations. It outperformed the empirical model in 45% of the test cases, with standout accuracy at low burnups (<1.1% FIMA), exemplified by CANEL 613-B (4% error) and CANEL 603-B (6% error). However, high burnup and extreme temperatures introduced greater uncertainty, as fission gas migration amplified errors (e.g., 220-B: 110% error). While the model maintained superior performance in select high-burnup scenarios, increasing fission gas migration and swelling at elevated burnups generally introduced greater uncertainty, underscoring the importance of the refinement of the gas diffusivity parameters in high-burnup and high-temperature regimes.

#### IV. MULTISCALE UQ OF URANIUM NITRIDE

At the next stage, further uncertainty reduction was achieved by applying Monte Carlo sampling to the key physical parameters (e.g., diffusion coefficients) that influence fuel swelling. In this work, the sampling distributions were either uniform or log-uniform depending on how many orders of magnitude the parameter space covered. This sampling was performed in a multiscale framework by coupling atomistic simulations using

calculations performed using ML interatomic potentials and DFT to the cluster dynamics code CENTIPEDE [36].

CENTIPEDE can be used to calculate the diffusivities of various chemical species and defects in the fuel lattice. The resulting data sets generated by CENTIPEDE serve as inputs to the updated mechanistic BISON models. Next, a calibration process was applied to the diffusion coefficient predictions. Baseline parameters in the cluster dynamics model, initially derived from DFT-derived and empirical potentials, can be calibrated self-consistently via a feedback loop integrating the data-driven methods (such as genetic algorithms), data augmentation techniques, molecular simulations, and experimental legacy data used for ML training [3]. The resulting data sets generated by CENTIPEDE serve as inputs to the mechanistic BISON models.

A principal step in the multiscale UQ process is to connect the atomistic-level calculations and simulations to the mesoscale diffusivity calculations by varying the parameters in the CENTIPEDE code, where each parameter represents a specific energetic or kinetic property in the fuel lattice. When performing CENTIPEDE calculations, the uncertainty in the atomistic parameters are explored by randomly sampling the values for each parameter within defined error bounds [38]. This sampling is done 5000 times, and a CENTIPEDE calculation is performed across multiple temperatures for each set of sampled parameters. The resulting temperature-dependent xenon and vacancy diffusivities are then fed

TABLE 1

SNAP-50 Test Series Operational Conditions and Model Uncertainty<sup>a</sup> [13,18,19]

| Test Series  | Capsule | Maximum Fuel Temperature (K) | Burnup (% FIMA) | Volumetric Swelling (vol %) |           |       | Error Differential (%) |       |
|--------------|---------|------------------------------|-----------------|-----------------------------|-----------|-------|------------------------|-------|
|              |         |                              |                 | Experimental                | Empirical | BISON | Empirical              | BISON |
| <b>CANEL</b> |         |                              |                 |                             |           |       |                        |       |
| 600          | T       | 1424                         | 0.19            | 3                           | 0.81      | 0.69  | -73%                   | -77%  |
|              | M       | 1551                         | 0.18            | 1.8                         | 0.94      | 0.80  | -48%                   | -56%  |
|              | B       | 1574                         | 0.18            | 1.8                         | 0.97      | 0.84  | -46%                   | -53%  |
| 602          | T       | 1272                         | 0.97            | 3                           | 2.34      | 2.09  | -22%                   | -30%  |
|              | M       | 1432                         | 0.91            | 3.5                         | 2.95      | 2.34  | -16%                   | -33%  |
|              | B       | 1399                         | 0.86            | 2.4                         | 2.65      | 2.18  | 10%                    | -9%   |
| 603          | T       | 1300                         | 0.74            | 2.9                         | 1.98      | 1.80  | -32%                   | -38%  |
|              | M       | 1460                         | 0.73            | 2.7                         | 2.58      | 2.08  | -5%                    | -23%  |
|              | B       | 1429                         | 0.71            | 2.1                         | 2.39      | 1.97  | 14%                    | -6%   |
| 613          | T       | 1388                         | 0.54            | 1                           | 1.79      | 1.53  | 79%                    | 53%   |
|              | M       | 1503                         | 0.53            | 1.4                         | 2.12      | 1.76  | 52%                    | 26%   |
|              | B       | 1413                         | 0.58            | 1.7                         | 1.98      | 1.63  | 16%                    | -4%   |
| 220          | T       | 1600                         | 0.95            | 5                           | 3.93      | 2.42  | -21%                   | -52%  |
|              | M       | 1800                         | 0.95            | 6                           | 5.2       | 5.01  | -13%                   | -17%  |
|              | B       | 1603                         | 0.96            | 1.9                         | 3.98      | 2.43  | 110%                   | 28%   |
| 231          | T       | 1741                         | 1.95            | 8.9                         | 8.74      | 5.02  | -2%                    | -44%  |
|              | M       | 1950                         | 1.92            | 10                          | 11.29     | 12.75 | 13%                    | 28%   |
|              | B       | 1810                         | 2.03            | 8.4                         | 9.92      | 6.57  | 18%                    | -22%  |
| 240          | T       | 1696                         | 1.51            | 5.8                         | 6.63      | 4.39  | 14%                    | -24%  |
|              | M       | 1800                         | 1.61            | 8                           | 8.04      | 7.76  | 0%                     | -3%   |
|              | B       | 1743                         | 1.58            | 7.8                         | 7.32      | 5.34  | -6%                    | -32%  |
| <b>ORNL</b>  |         |                              |                 |                             |           |       |                        |       |
| 658          | T       | 1428                         | 1.08            | 3.7                         | 3.36      | 2.64  | -9%                    | -29%  |
|              | M       | 1502                         | 1.08            | 3.8                         | 3.78      | 3.22  | 0%                     | -15%  |
|              | B       | 1485                         | 1.08            | 3.5                         | 3.68      | 3.01  | 5%                     | -14%  |
| 662          | T       | 1383                         | 1.16            | 4.1                         | 3.3       | 2.60  | -20%                   | -37%  |
|              | M       | 1519                         | 1.16            | 4.3                         | 4.12      | 3.57  | -4%                    | -17%  |
|              | B       | 1514                         | 1.16            | 4.5                         | 4.09      | 3.48  | -9%                    | -23%  |
| 664          | T       | 1418                         | 0.58            | 1.8                         | 1.98      | 1.81  | 10%                    | 1%    |
|              | M       | 1457                         | 0.58            | 1.4                         | 2.11      | 1.98  | 51%                    | 41%   |
|              | B       | 1480                         | 0.58            | 1.2                         | 2.19      | 2.12  | 83%                    | 77%   |
| 665          | T       | 1327                         | 4.58            | 7.1                         | 9.23      | 5.28  | 30%                    | -26%  |
|              | M       | 1432                         | 4.58            | 7.9                         | 11.05     | 5.74  | 40%                    | -27%  |
|              | B       | 1377                         | 4.58            | 7.7                         | 10.07     | 5.50  | 31%                    | -29%  |
| 667          | T       | 1434                         | 0.78            | 3                           | 2.6       | 2.16  | -13%                   | -28%  |
|              | M       | 1489                         | 0.78            | 1.7                         | 2.84      | 2.46  | 67%                    | 45%   |
|              | B       | 1505                         | 0.78            | 1.8                         | 2.91      | 2.57  | 62%                    | 43%   |
| 669          | T       | 1213                         | 2.72            | 6.1                         | 4.87      | 3.56  | -20%                   | -42%  |
|              | M       | 1354                         | 2.72            | 6.9                         | 6.31      | 4.04  | -8%                    | -41%  |
|              | B       | 1314                         | 2.72            | 5.6                         | 5.88      | 3.91  | 5%                     | -30%  |

<sup>a</sup>(+) uncertainty values indicate swelling values are greater than experimental

(-) uncertainty values indicate model values are less than experimental.

<sup>b</sup>T (top capsule), M (middle capsule), and B (bottom capsule).

into BISON, where fuel behavior is simulated for each of the 5000 sets of sampled atomic-scale parameters.

Shown in Fig. 5 are the diffusivity distributions for xenon-based defects and vacancy-based defects at 1000 K and 1800 K, respectively, calculated using the baseline atomistic parameters calculated using DFT and empirical methods [38]. The orange curve in each plot is a fit of the data to a skew-normal distribution. The temperature-dependent diffusivity curves used in BISON are shown in Fig. 6.

Compare the distributions in Fig. 5 to those shown in Fig. 7, which include the information from ML interatomic potentials for UN developed by us, which to our knowledge, are the first ML-based potentials for UN [6]. The ML potentials reduce the variance in the distributions compared to the baseline parameter set. This can be seen by comparing the variance for each distribution in each of the two figures. In each plot, the skew-normal fitting usually fits the data well, but for the more sharply peaked symmetric distributions (Xe at 1000 K) and highly asymmetric distributions (vacancies at 1000 K), the fit does not quantitatively capture the distribution behavior, though they are qualitatively reasonable.

A log-normal fitting was also attempted, and its performance was significantly worse than skew normal.

The effect the ML method had on the variance and skew of these fits compared to the DFT data is shown by comparing Figs. 5 and 7.

Fig. 8 shows how the impact of reducing atomistic uncertainties can affect uncertainties in the diffusivity calculations in a hypothetical situation where the error bounds on the atomistic parameters have been reduced by a factor of 10. The baseline distributions are shown in purple, and the new distributions after uncertainty reduction are shown in red. Notice that reducing the atomistic uncertainties by an order of magnitude results in several orders of magnitude reduction in the variance of the diffusivity distributions. This nonlinear relation between uncertainty input and uncertainty output could be an important observation affecting multiscale AFQ processes.

At the reactor scale, BISON predicts behaviors like fuel swelling. To do this, some of the mesoscale parameters it requires are the diffusivities of xenon defects and vacancies. Here, these diffusivities and other mesoscale properties were obtained via CENTIPEDE; but CENTIPEDE requires atomic-scale parameters for each chemical species present as inputs.

By integrating diffusivity uncertainties, developed through the methodologies previously described, with burnup variations, we further identified and refined key uncertainties affecting UN fuel swelling, as illustrated in

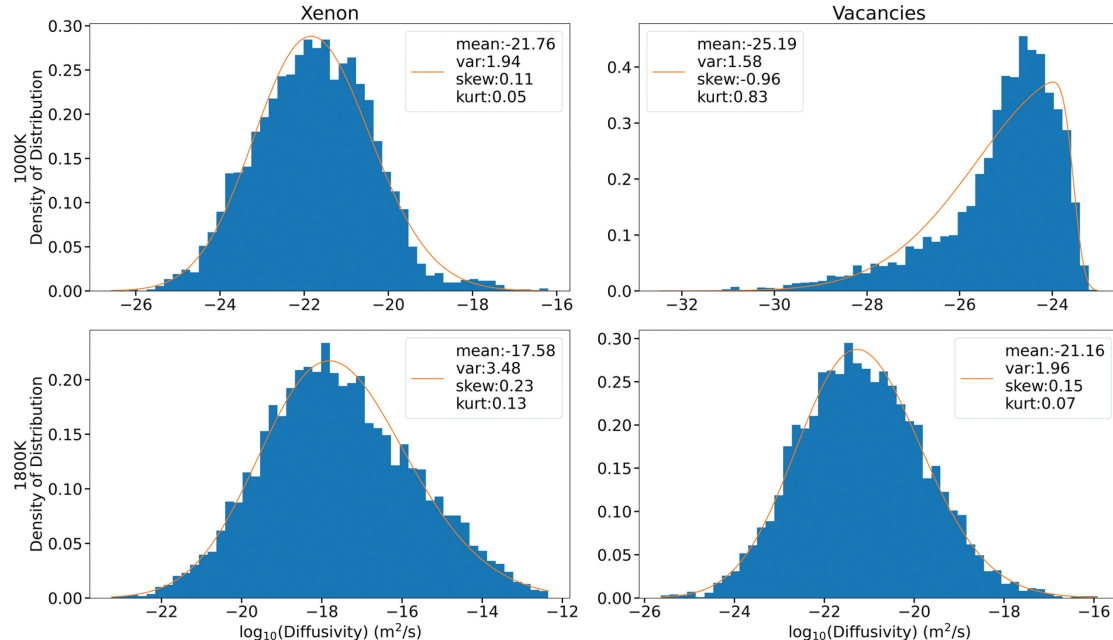


Fig. 5. Diffusivity distributions of (left) xenon-based defects and (right) vacancy-based defects in UN calculated using CENTIPEDE with input data from DFT calculations and empirical methods [38]. The top row is for 1000 K and the bottom row is for 1800 K. The orange curve in each plot is a fit to a skew-normal distribution with the respective distribution parameters shown in each legend.

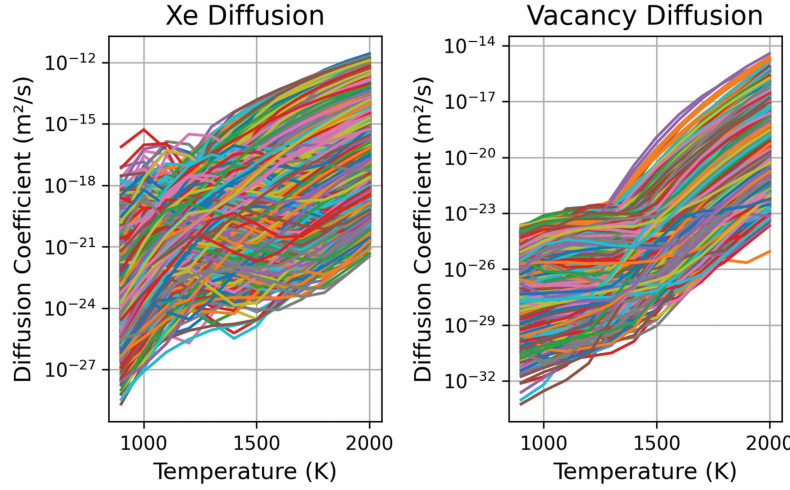


Fig. 6. Temperature-dependent diffusivity curves for (left) xenon and (right) vacancies. Each curve represents the results of a different parameter set used in CENTIPEDE.

**Fig. 9.** The diffusion rates of the defects, including xenon, uranium, and nitrogen, play a critical role in swelling behavior [3]. This was demonstrated by generating a series of temperature-dependent diffusivity curves derived from random sampling within known uncertainty bounds for various input parameters within the DFT simulations [3].

From these random distributions of Xe and U diffusivity, we generated corresponding distributions of fuel pin diameter changes, exemplifying the impact of

diffusivity variability. The left panel of **Fig. 9** presents fuel pin diameter predictions as a function of burnup, showing distributions of predicted values at each burnup step due to the random diffusivity distributions.

The width of the distributions increases with burnup because the contribution from gaseous products increases, and as a result, impact on the fuel pin diameter from the diffusion rates becomes more significant. For low burnup, the impact is low and the distribution is narrow and peaked. The

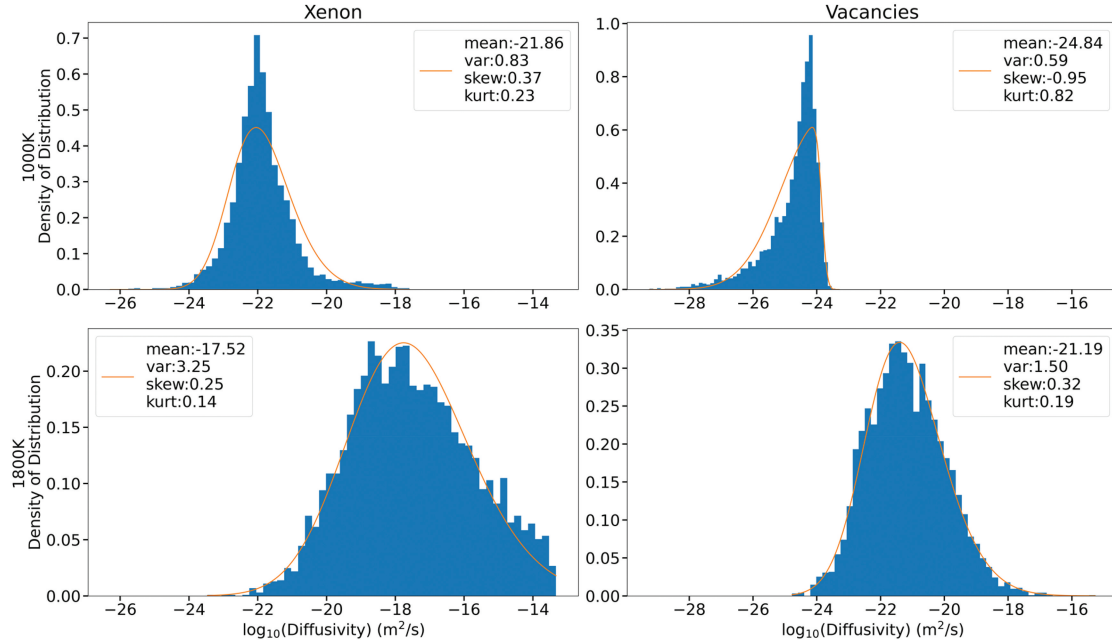


Fig. 7. Diffusivity distributions of (left) xenon-based defects and (right) vacancy-based defects in UN calculated using CENTIPEDE with input parameters generated from a ML interatomic potential [6]. The top row is for 1000 K and the bottom row is for 1800 K. The orange curve in each plot is a fit to a skew-normal distribution with the respective distribution parameters shown in each legend.

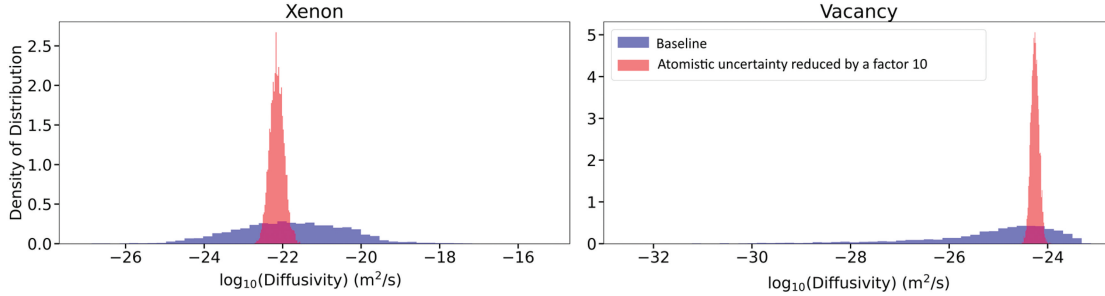


Fig. 8. Idealized case showing the diffusivity distributions using the baseline error bounds on the atomistic parameters (blue) compared to the case when those bounds are reduced by a factor of 10. All CENTIPEDE simulations used to generate these results were performed at 1000 K.

impact from gaseous products below 0.8% FIMA is negligible, as expected, based on past experiments and theory.

Additionally, the fuel pin diameter grows with increases in burnup and with increases in temperature (not shown on the graph). The table on the right side of Fig. 9 shows a comparison between the empirical and mechanistic BISON model predictions of the fuel pin diameters and corresponding uncertainties. The fuel pin diameters resulting from the correlation-based empirical model were smaller than the diameters calculated using the mechanistic model. The difference between the two methods increased with burnup, with the contribution of gaseous swelling to the diameter increasing. This indicated that the correlation-based model did not capture the physics and underestimated the fuel pin diameter.

Consequently, its use requires the utilization of higher safety margins with the corresponding additional constraints on the power plant. Also, the uncertainties associated with the empirical model were larger (25% to 60%) due to the uncertainties in the corresponding experimental data. At the next step, it is planned to model the burnup in the range of 3% to 8% FIMA

using better statistics and to compare to the experimental series BR-10 that was not used in the development of the BISON mechanistic model.

Also, although not performed in this work, the final uncertainty reduction in the performance envelope of the nuclear fuel, in this case UN, can result from the generation of new experimental ion irradiation data. This new data will be used to validate predictions of dislocation and fission gas behavior as functions of temperature and fluence generated by the mechanistic swelling models. These experiments will target physical regimes with the highest uncertainty as calculated using the multiscale framework presented in this work.

## V. UN FUEL PERFORMANCE ENVELOPE

The fuel performance envelope defines the environmental conditions and radiation exposure under which nuclear fuel must reliably perform [2]. It supports safety analysis and informs the design of the reactor core, fuel assemblies, and operating limits. The fuel performance

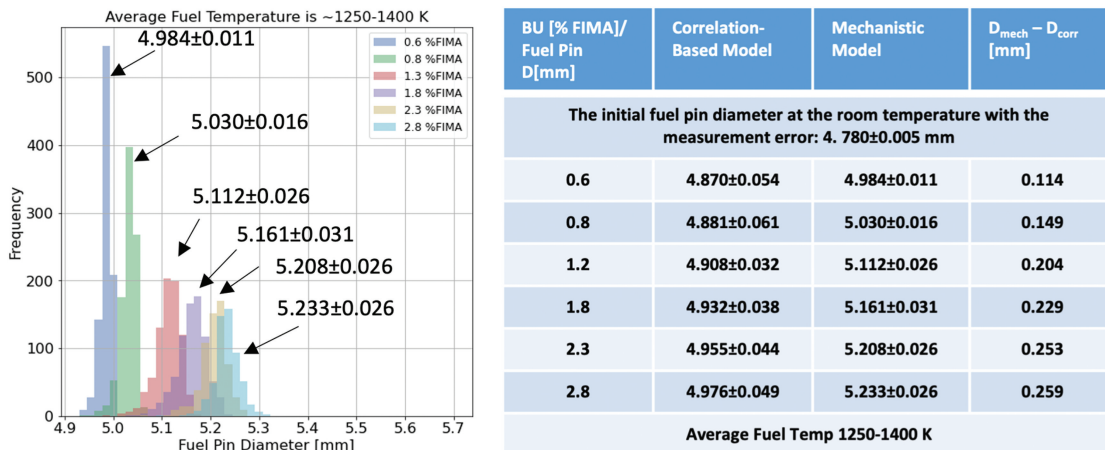


Fig. 9. Fuel pin diameter prediction using the (left) new mechanistic model and (right) a comparison to the old empirical model.

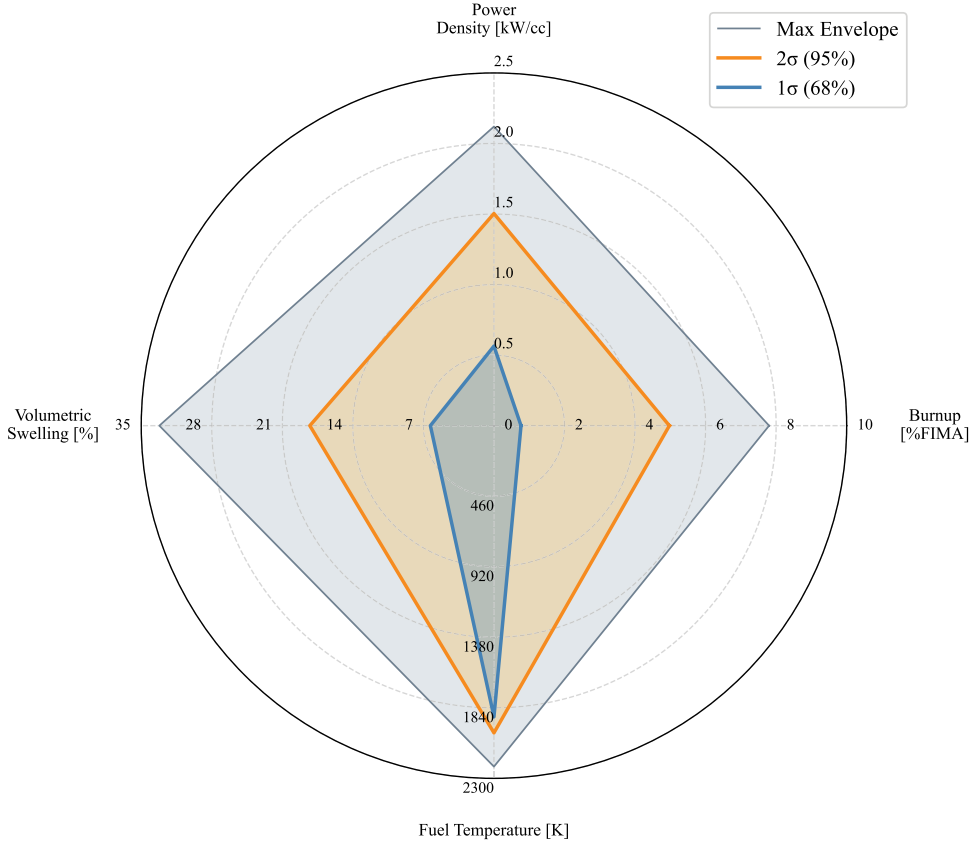


Fig. 10. Initial UN fuel performance envelope based only on past experimental data [14–37]. The gray outline corresponds to all available data, orange is the 95th percentile, and blue is the 68th percentile.

envelope significantly influences the broader nuclear power plant operating envelope, including key parameters such as fuel temperature, power peaking, and coolant temperature. It also affects technical factors like cycle length, target burnup, and refueling strategy.

To construct an initial performance envelope for UN fuel, all available legacy volumetric swelling data were plotted as a function of maximum fuel temperature, power density, and burnup. This envelope defines the parameter space where experimental data currently exist, providing a reference for comparison with other data, such as the mechanistic fuel performance model predictions.

Within this envelope, three boundaries are highlighted in Fig. 10. The gray region encompasses the full range of raw data. The orange outline indicates the upper bound of the  $2\sigma$  (95%) envelope, and the blue outline shows the  $1\sigma$  (68%) envelope. Together, these define the space where the available data, and thus confidence in UN fuel performance predictions, is highest.

BISON was employed to evaluate UN fuel performance, incorporating advanced mechanistic approaches. Past experimental data were statistically

analyzed and compared to the simulation results from BISON to validate the model predictions. Fig. 11 shows a side-by-side comparison of the performance envelope of the SNAP-50 irradiation data compared to the same test pins analyzed through the BISON mechanistic fuel performance code. The maximum envelope maintains an approximate shape; however, the 1 and 2 sigma volumetric swelling reduce in size when using the BISON fuel performance model. This indicated that the model tended to underpredict the upper percentile values ( $1\sigma$  and  $2\sigma$ ), resulting in a narrower predicted performance envelope compared to experimental observations. Further validation against a broader set of experimental data is recommended to ensure the model accurately captures the full range of fuel performance.

To continue revising the fuel performance envelope shown in Fig. 11, the full uncertainty reduction methodology outlined in Fig. 2, along with analysis of operating transients in a generic microreactor, are required. Additionally, it is anticipated that this envelope will be expanded through new experiments guided by PIRT analyses specific to unique reactor designs.

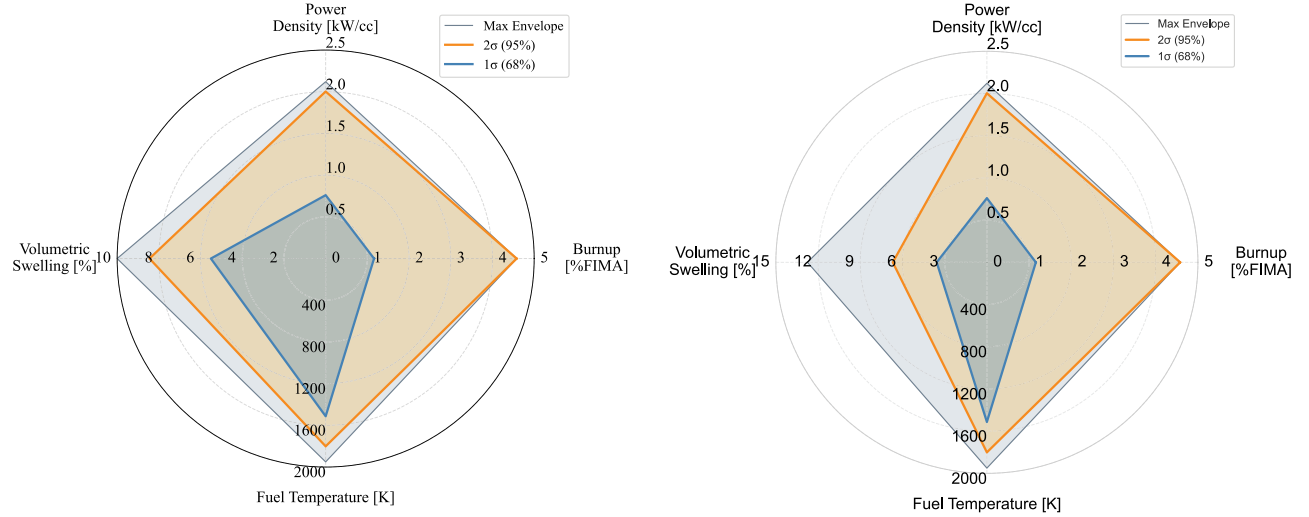


Fig. 11. Initial UN fuel performance envelope based only on SNAP-50 experimental data [18,19]: (left) SNAP-50 irradiation data and (right) BISON fuel performance results. The gray outline corresponds to all available data, orange is the 95th percentile, and blue is the 68th percentile.

These experiments will be informed by the completed AFQ work, which identified the dominant phenomena influencing UN fuel behavior. Each reactor vendor is expected to tailor and extend the fuel performance envelope based on PIRT analyses relevant to their design and by leveraging the AFQ methodology. This will ensure that performance predictions are reliable across a broader range of conditions.

## VI. CONCLUSIONS

Advanced fuels are supported by a limited set of experimental data, which falls short of meeting the requirements for traditional fuel qualification processes. Recognizing this gap, there is growing interest in developing AFQ methodologies. In this work, we presented the development of a prototype AFQ framework designed to address these challenges. This framework integrates advanced modeling, ML techniques, legacy experimental data, and a select set of new experiments to systematically investigate potential failure mechanisms in UN fuel.

We detailed the structure of the proposed framework and its application to UN fuel characterization. Notably, we reported initial predictions of UN swelling, a key life-limiting failure mode for uranium nitride fuel, along with the associated computational uncertainties. The AFQ approach demonstrated improved accuracy in predicting fuel pin diameter changes and achieved a reduction in uncertainty compared to previous methods.

The preliminary fuel performance envelope, based on swelling as a function of fuel temperature, power density, and burnup, was first established using historical experimental data. This envelope, refined with new multiphysics modeling, will be updated again with UQ derived from the developed multiscale AFQ framework in the future. Overall, our findings provided evidence that multiscale UQ, facilitated by ML, can effectively narrow the safe performance envelope for UN fuel, offering a robust and data-driven pathway for advanced fuel qualification.

## Author Contributions

CRediT: **Zachary Miller:** Investigation, Methodology, Writing – review & editing; **Landon Johnson:** Investigation, Methodology; **Lorena Alzate-Vargas:** Investigation, Methodology; **Jason Rizk:** Formal analysis, Investigation, Methodology; **Christopher Matthews:** Formal analysis, Investigation, Methodology; **Michael W. D. Cooper:** Investigation, Methodology; **Vedant Mehta:** Investigation; **David A. Andersson:** Investigation, Methodology, Supervision; **Galen T. Craven:** Investigation, Methodology, Writing – review & editing; **Massimiliano Fratoni:** Supervision; **Alex Levinsky:** Conceptualization, Investigation, Methodology, Supervision, Writing – original draft.

## Disclosure Statement

No potential conflict of interest was reported by the author(s).

## Funding

This research was in part supported by the Laboratory Directed Research and Development program of Los Alamos National Laboratory (LANL) under project number [20220053DR], “Accelerating Nuclear Fuel Qualification Through Integrated Multiscale and Multiphysics Models.” This work was supported by the U.S. Department of Energy (DOE) through LANL. LANL is operated by Triad National Security, LLC, for the National Nuclear Security Administration of the DOE [contract no. 89233218CNA000001]. This paper is approved for unlimited release under LA-UR-23-33681.

## References

1. Z. A. Miller et al., “Uranium Mononitride (UN) Handbook,” LA-UR-24-29668, Los Alamos National Laboratory (2024).
2. “Fuel Qualification for Advanced Reactors,” NUREG-2246, U.S. Nuclear Regulatory Commission (Mar. 2022).
3. G. T. Craven et al., “Data-Driven Methods for Diffusivity Prediction in Nuclear Fuels,” *Comput. Mater. Sci.*, **230**, 112442 (2023); <https://doi.org/10.1016/j.commatsci.2023.112442>.
4. J. T. Rizk et al., “Mechanistic Nuclear Fuel Performance Modeling of Uranium Nitride,” *J. Nucl. Mater.*, **606**, 155604 (2025).
5. L. Johnson et al., “Machine Learning Method to Determine Concentrations of Structural Defects in Irradiated Materials,” *Comput. Mater. Sci.*, **242**, 113079 (2024).
6. L. Alzate-Vargas et al., “Toward Machine Learning Interatomic Potentials for Modeling Uranium Mononitride,” *Machine Learning: Science and Technology* 6 (3), 035064 (2025).
7. R. Chen et al., “Machine Learning Models for Volumetric Swelling in Uranium Nitride,” *J. Nucl. Mater.*, **615**, 155980 (2025).
8. M. R. Tonks et al., “Mechanistic Materials Modeling for Nuclear Fuel Performance,” *Ann. Nucl. Energy*, **105**, 11 (2017); <https://doi.org/10.1016/j.anucene.2017.03.005>.
9. M. R. Tonks et al., “Assessment of MARMOT: A Mesoscale Fuel Performance Code,” INL/EXT-15-35108, Idaho National Laboratory (Apr. 2015).
10. R. B. Matthews, “Irradiation Performance of Nitride Fuels,” LA-UR-93-2392, Los Alamos National Laboratory (1993).
11. S. I. Porollo et al., “Analysis of Experimental Data on Gas Release and Swelling of UN Fuel Irradiated in BR-10 Reactor,” IAEA-CN245-081, International Atomic Energy Agency (2016).
12. R. L. Williamson et al., “Multidimensional Multiphysics Simulation of Nuclear Fuel Behavior,” *J. Nucl. Mater.*, **423**, 1, 149 (2012); <https://doi.org/10.1016/j.jnucmat.2012.01.012>.
13. S. B. Ross, M. S. El-Genk, and R. B. Matthews, “Uranium Nitride Fuel Swelling Correlation,” *J. Nucl. Mater.*, **170**, 2, 169 (1990); [https://doi.org/10.1016/0022-3115\(90\)90409-G](https://doi.org/10.1016/0022-3115(90)90409-G).
14. L. M. Zabudko and V. M. Poplavsky, “Investigations of Nitride Fuels for Fast Reactors in Russia,” *Proceedings of the symposium on nitride fuel cycle technology*, JAERI-CONF-2004-015, Japan Atomic Energy Research Institute (2004).
15. S. I. Porollo and S. N. Ivanov, “Corrosion Damage and Mechanical Properties of BR-10 Reactor Fuel-Rod Cladding with Mononitride Uranium Fuel,” *At. Energy*, **125**, 185 (2019).
16. S. I. Porollo et al., “Analysis of Experimental Data on Gas Release and Swelling of UN Fuel Irradiated in BR-10 Reactor,” International Atomic Energy Agency (2016).
17. S. S. Voss, “SNAP (Space Nuclear Auxiliary Power) Reactor Overview,” Air Force Weapons Laboratory, Kirtland Air Force Base (1984).
18. S. C. Weaver and J. L. Scott, “Comparison of Reactor Fuels for High Temperature Applications,” ORNL-TM\_1360, Oak Ridge National Laboratory (1965).
19. M. A. DeCrescente, M. S. Freed, and S. D. Caplow, “Uranium Nitride Fuel Development, SNAP-50,” PWAC-488, Pratt and Whitney Aircraft, Middletown, Connecticut, Connecticut Advanced Nuclear Engineering Laboratory (1965).
20. S. C. Weaver et al., “Effects of Irradiation on Uranium Nitride Under Space-Reactor Conditions,” ORNL-4461, Oak Ridge National Laboratory (1969).
21. R. E. Gluyas and G. K. Watson, “Materials Technology for an Advanced Space Power Nuclear Reactor Concept: Program Summary,” E-7893, U.S. National Aeronautics and Space Administration (1975).
22. R. E. Gluyas and A. F. Lietzke, “Materials Technology Program for a Compact Fast Reactor for Space Power,” NASA-TM-X-67869, U.S. National Aeronautics and Space Administration (1971).
23. R. G. Rohal, T. N. Tambling, and R. L. Smith, “Testing of Uranium Nitride Fuel in T-111 Cladding at 1200 K Cladding Temperature,” E-7192, U.S. National Aeronautics and Space Administration (1973).
24. J. G. Slaby et al., “Irradiation of Three T-111 Clad Uranium Nitride Fuel Pins for 8070 Hours at 990 C (1815 F),” NASA-TM-X-2878, U.S. National Aeronautics and Space Administration (1973).
25. K. J. Bowles and R. E. Gluyas, “Evaluation of Refractory-Metal-Clad Uranium Nitride and Uranium

Dioxide Fuel Pins After Irradiation for Times Up to 10450 Hours at 990 C,” NASA-TN-D-7891, U.S. National Aeronautics and Space Administration (1975).

26. J. G. Slaby and B. L. Siegel, “Examination of T-111 Clad Uranium Nitride Fuel Pins Irradiated Up to 13,000 Hours at a Clad Temperature of 990C,” E-7579, U.S. National Aeronautics and Space Administration (1973).

27. R. G. Rohal and T. N. Tambling, “Unrestrained Swelling of Uranium-Nitride Fuel Irradiated at Temperatures Ranging from 1100 to 1400 K (1980 to 2520 R),” E-7464, U.S. National Aeronautics and Space Administration (1973).

28. S. F. Demuth, “SP100 Space Reactor Design,” *Prog. Nucl. Energy*, **42**, 3, 323 (2003).

29. D. S. Dutt et al., “Performance Testing of Refractory Alloy-Clad Fuel Elements for Space Reactors,” HEDL-SA-3347-FP; CONF-850808-25, Hanford Engineering Development Laboratory, Richland, Washington (1985).

30. R. A. Karnesky and R. E. Mason, “Post-Irradiation Examination Results from SP-1,” HEDL-SA-3391; CONF-860102-15, Hanford Engineering Development Laboratory, Richland, Washington (1986).

31. R. B. Matthews et al., “Fabrication and Testing of Uranium Nitride Fuel for Space Power Reactors,” *J. Nucl. Mater.*, **151**, 3, 345 (1988).

32. B. J. Makenas et al., “SP-100 Fuel Pin Performance: Results from Irradiation Testing,” *AIP Conf. Proc.*, **301**, 1 (1994).

33. B. J. Makenas, J. W. Hales, and A. L. Ward, “Fuels Irradiation Testing for the SP-100 Program,” *AIP Conf. Proc.*, **217**, 2 (1991).

34. D. L. Keller, “Progress in Development of Fuels and Technology for Advanced Reactors During July, 1969, Through June, 1970,” Annual Report BMI-1886, Battelle Memorial Institute (1970).

35. D. L. Keller, “Progress in Development of Fuels and Technology for Advanced Reactors During July through September 1970,” Annual Report BMI-1893, Battelle Memorial Institute (1970).

36. D. L. Keller, “Progress in Development of Fuels and Technology for Advanced Reactors During October through December 1970,” Annual Report BMI-1898, Battelle Memorial Institute (1970).

37. D. L. Keller and W. Chubb, “Progress in Development of Fuels and Technology for Advanced Reactors During August, 1967, Through July 1968,” Annual Report BMI-1848, Battelle Memorial Institute (1968).

38. M. W. D. Cooper et al., “Simulations of Self- and Xe Diffusivity in Uranium Mononitride Including Chemistry and Irradiation Effects,” *J. Nucl. Mater.*, **587**, 154685 (2023).